Chemistry–A European Journal
Research Article
doi.org/10.1002/chem.202300979
Chemistry Europe
European Chemical Societies Publishing

www.chemeurj.org

Novel Method for the Synthesis of Merocyanines: New Photophysical Possibilities for a Known Class of Fluorophores

Brunella Bardi[+],[a] Katerina V. Vygranenko[+],[b] Beata Koszarna,[b] Olena Vakuliuk,[b] Łukasz Dobrzycki,*[c] Daniel T. Gryko,*[b] Francesca Terenziani,*[a] and Anna Painelli[a]

Abstract: A new, transformative method for the preparation of rhodols and other merocyanines from readily available tetrafluorohydroxybenzaldehyde and aminophenols has been developed. It is now possible to prepare merocyanines bearing three fluorine atoms and additional conjugated rings, and the whole one-pot process occurs under neutral, mild conditions. Three heretofore unknown merocyanine-based architectures were prepared using this strategy from aminonaphthols and 4-hydroxycoumarins. The ability to change the structure of original rhodol chromophore into π-expanded merocyanines translates to a comprehensive method for the modulation of photophysical properties, such as shifting the absorption and emission bands across almost the entire visible spectrum, reaching a huge Stokes shift i.e. 4800 cm^{-1}, brightness approximately 80.000 M^{-1} cm^{-1}, two-photon absorption cross-section above 150 GM and switching-on/off solvatofluorochromism. A detailed investigation allowed to rationalize the different spectroscopic behavior of rhodols and new merocyanines, addressing solvatochromism and two-photon absorption.

Introduction

Rhodamines, fluoresceins and rhodols are iconic fluorophores which, although developed in the 19th century, are still popular objects of research,[1] because of their large brightness combined with their straightforward preparation. The synthesis from phenols/aminophenols and phthalic anhydride, however, limited the studies on the relationship between the structure of these dyes and their photophysical properties to substituents at position 9 (see numbering in Scheme 1). During the last two decades, the second bridging atom, i.e. oxygen, was replaced with silicon,[2–4] phosphorus,[5,6] sulfur,[7] or carbon[8–10] in rhodamine,[11–14] fluorescein,[15,16] and rhodol[17] scaffolds or it was removed entirely,[18] with spectacular success in terms of bathochromic shift of fluorescence and increased stability. The remaining positions 1, 2, 4, 5, 7 and 8 were dormant, although in Alexa-type fluoresceins two fluorine atoms are inserted at the left ring, featuring increased stability.[19] Vygranenko et al. have recently proposed a novel strategy showing that the reaction of 3-formyl-7-dialkylaminocoumarins with dimethyl ketoglutarate leads to the formation of rhodols in one step, which possess CO_2Me substituents at positions 2 and 4.[20]

Here we report an even simpler methodology leading to rhodols with three fluorine atoms at positions 1, 2 and 4. It is well-known that activated fluoroarenes undergo nucleophilic aromatic substitution with phenols,[21] as well as aromatic aldehydes react with 3-dialkylaminophenols or other electron-rich aromatics.[22–24] Performing these two steps simultaneously can in principle lead to the formation of a six-membered ring bridging two benzene rings in a linear fashion, opening the possibility to devise an entirely new retrosynthetic pathway towards xanthene dyes. We show this new concept with the synthesis of a library of trifluororhodols and related π-expanded merocyanines, and compare their photophysics with rhodols characterized by different electron-withdrawing substituents, specifically two ester groups.[20] Extensive spectroscopic characterization revealed interesting differences between rhodols and merocyanines, which were fully rationalized through in-depth computational investigation and theoretical modeling.

[a] *Dr. B. Bardi,[+] Prof. F. Terenziani, Prof. A. Painelli*
Department of Chemistry, Life Sciences and Environmental Sustainability
University of Parma
Parco Area delle Scienze 17/a, 43124 Parma (Italy)
E-mail: francesca.terenziani@unipr.it

[b] *K. V. Vygranenko,[+] Dr. B. Koszarna, Dr. O. Vakuliuk, Prof. D. T. Gryko*
Institute of Organic Chemistry Polish Academy of Sciences
Warsaw (Poland)
E-mail: dtgryko@icho.edu.pl

[c] *Prof. Ł. Dobrzycki*
Faculty of Chemistry
University of Warsaw
Żwirki i Wigury 101, 02-089 Warsaw (Poland)
E-mail: dobrzyc@chem.uw.edu.pl

[+] *These authors contributed equally to this work.*

Supporting information for this article is available on the WWW under https://doi.org/10.1002/chem.202300979

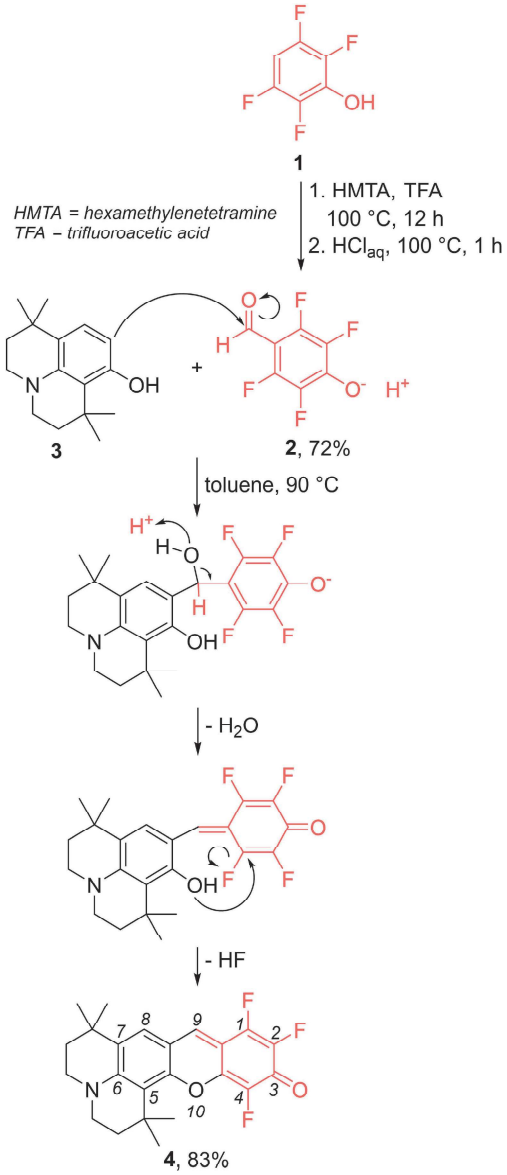

Scheme 1. Synthesis of rhodol **4**.

Results and Discussion

Design and synthesis

In the envisioned synthetic strategy, we have chosen 3-dialkylaminophenol as the model substrate. On the other hand, the second molecule, besides being 2-fluorobenzaldehyde, must consider three strict requirements: (1) the reactivity of the formyl group will be enhanced by the presence of four moderately electron-withdrawing fluorine atoms; (2) the reactivity of the C–F bonds towards nucleophilic aromatic substitution will be enhanced by the electron-withdrawing CHO group; (3) the strategically placed OH group will become rhodol's C=O functionality. Their combination points towards 4-hydroxybenzaldehyde possessing four fluorine atoms.

Consequently the project started with the synthesis of 4-hydroxy-2,3,5,6-tetrafluorobenzaldehyde (**2**) from tetrafluorophenol (**1**) via a Duff reaction,[25–27] (Scheme 1). As outlined earlier, we designed the new approach towards rhodols based on a combination of the Friedel–Crafts reaction and an aromatic nucleophilic substitution of a fluorine atom. Our initial experiments revealed that simply heating of 2,3,5,6-tetrafluoro-4-hydroxybenzaldehyde (**2**) with 8-hydroxy-1,1,7,7-tetramethyljulolidine (**3**) in toluene leads to the formation of the targeted rhodol **4**.

The novel rhodol **4** was used as a model for further investigation and optimization of the reaction conditions. When the reaction was carried out in toluene at 60 °C, product **4** was obtained in low yield and with a sizable amount of unidentified side-products (Table 1, entry 1).

The first factor we decided to investigate was temperature. Increasing the reaction temperature significantly improved the yield of dye **4** and shortened the reaction time (Table 1, entry 2). Further increase of the reaction temperature to reflux (i.e. 110 °C) led to the formation of a higher number of side-products which hampered the purification (Table 1, entry 3). Since the first step of the studied transformation is an electrophilic aromatic substitution, we have selected two Lewis acids known for their efficiency as catalysts in Friedel–Crafts acylation and alkylation, namely aluminum(III) chloride and scandium(III) triflate.[28–30] The reaction performed in the presence of $AlCl_3$ and $Sc(OTf)_3$ led however to slightly lower yield of rhodol **4** (Table 1, entries 4–5). Our next move resulted from the combination of the following arguments: (a) the second step, i.e. nucleophilic aromatic substitution would benefit from the presence of a base; (b) reactions of reactive aldehydes with strongly electrophilic partners are known to occur in the presence of bases.[31] We found that the addition of sterically hindered 2,4,6-tri(*tert*-butyl)pyridine[32] did not affect the reaction yield (Table 1, entry 6), whereas strong non-nucleophilic phosphazene-type base stopped the reaction (Table 1, entry 7). Replacement of toluene with other solvents, such as DMSO (polar, aprotic), THF (moderately polar, aprotic) and hexafluoroisopropanol (HFIP) (polar, protic, slightly acidic) led to detrimental results (Table 1,

Table 1. Conditions for the optimization of the condensation of aldehyde **2** with phenol **3**.

Entry	solvent	T / °C	catalyst	time / h	yield
1	toluene	60	none	12	37%
2	toluene	90	none	1	83%
3	toluene	reflux	none	1	77%
4	toluene	90	$AlCl_3$	1	68%
5	toluene	90	$Sc(OTf)_3$	1	70%
6	toluene	90	2,4,6-tri-*tert*-butylpyridine	1	78%
7	toluene	90	phosphazene base P_1-t-Bu	1	trace
8	DMSO	80	none	1	11%
9	THF	60	none	12	24%
10	HFIP	80	none	1	0%
11	mesitylene	reflux	none	1	75%
12	xylenes	135	none	1	81%

entries 8–10). Finally, the higher-boiling analogs of toluene turned out not to be better solvents than toluene for the formation of rhodol **4** (Table 1, entries 11–12). The optimization process brought us to the conclusion that the conversion of the aminophenols into the corresponding rhodols shows the best outcome in nonpolar solvents at high temperature without any catalyst. In all probability the process starts from the Friedel–Crafts alkylation of electron-rich phenol **3** by the formyl group, with H^+ originating from highly acidic phenol **2** as possible catalyst. Once the carbon-carbon bond is formed, an intramolecular S_NAr reaction occurs with elimination of weakly acidic HF.

To test the synthetic utility of the optimized reaction conditions, we employed various aminophenols. Rhodols **11–14** were prepared in 31–87% yield (Scheme 3).

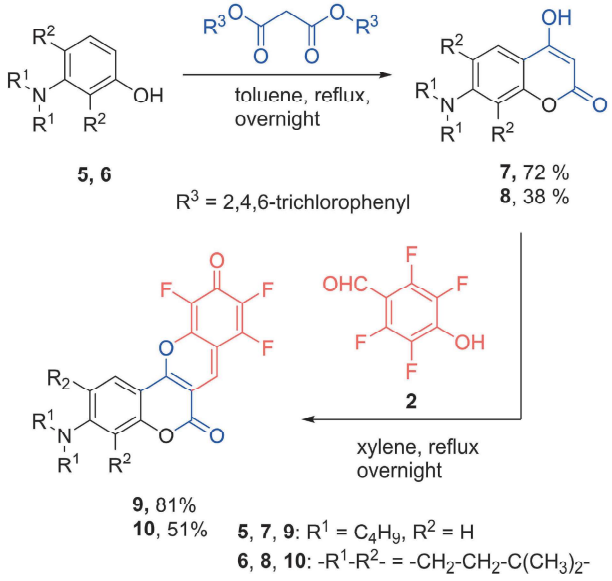

Scheme 2. Synthesis of coumarins **7**, **8** and their transformation into the corresponding merocyanines **9** and **10**.

Recognizing that the biggest advantage of the new methodology can lie in forging an access to heretofore non-existing rhodol-type fluorophores, we subsequently employed 4-hydroxy-7-dialkylaminocoumarins (Scheme 2 and 3). During the scope and limitations studies, it turned out that condensation of 4-hydroxycoumarins **7** and **8** with aldehyde **2** produces hybrid coumarino-merocyanines **9** and **10** with very poor yield due to the slow conversion of the intermediate products into the desired rhodols. For this reason, we replaced toluene with xylenes (hence we increased reaction temperature) in order to achieve higher conversion and reasonable yields of dyes **9** and **10**. This result was attributed to the fact that 4-hydroxycoumarins **7** and **8** do not belong to phenols, and consequently their reactivity towards both electrophilic aromatic substitution and nucleophilic substitution is different.

The new methodology enabled, for the first time, the synthesis of an unprecedented linear rhodol-type merocyanines, whose photophysical properties could be compared with those of the angular one. First, we have synthesized 7-(dihexylamino)naphthalen-2-ol (**S1**) and subjected it to condensation with aldehyde **2** in xylenes for 7 h (see Supporting Information Scheme S1). We have obtained only the angular merocyanine **15**, because position 1 of derivative **S1** is much more reactive than position 3. The use of naphthalene precursor **S5** with blocked position 1 enabled a selective reaction leading to a linear product (see Supporting Information Scheme S2). The substrate was prepared by condensation of diisopropylamine with 2,7-dihydroxynaphthalene under Bucherer conditions, followed by alkylation of the hydroxy group with allyl bromide and Claisen rearrangement. Reduction of the double bond with the Pd catalyst in the hydrogen atmosphere led to the formation of the precursor of merocyanine **16**.

Due to the poor reactivity of the 3-position of naphthalene, we were forced to increase condensation time (72 h) and temperature (xylenes, 160 °C). The desired dye **16** was obtained with 10% yield as dark blue crystals. Its structure has been confirmed by X-ray crystallography (ESI, CCDC 2250222).

Deposition Number 2250222 contains the supplementary crystallographic data for this paper. These data are provided free of charge by the joint Cambridge Crystallographic Data

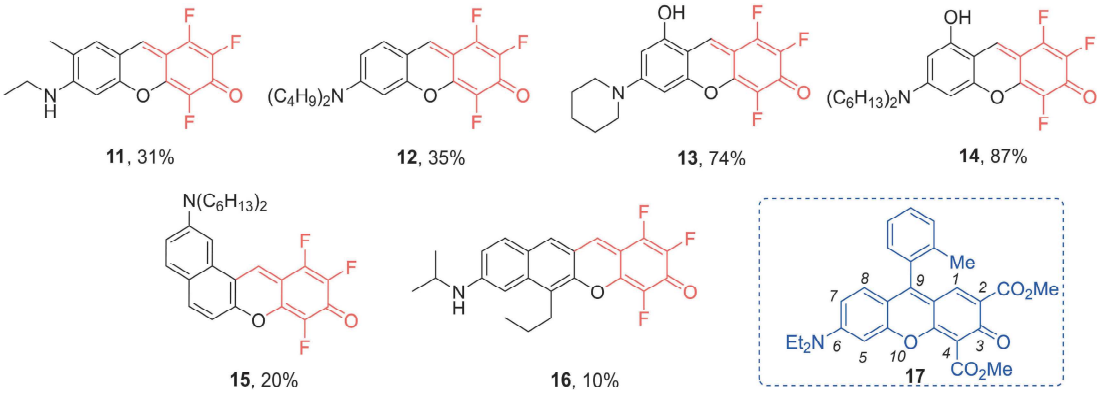

Scheme 3. Synthesized rhodols and merocyanines, as well as the molecular structure of the "reference" rhodol **17**, together with position numbering.

Centre and Fachinformationszentrum Karlsruhe Access Structures service.

Spectroscopic characterization

The linear absorption and emission spectra of rhodols **4**, **11–14** and **17** and merocyanines **9**, **10**, **15** and **16** were collected in different solvents, spanning a wide range of polarities. The main spectroscopic data are summarized in Table 2 and S12, while spectra of selected dyes are presented in Figure 1 (spectra of the other compounds can be found in Figure S2).

Absorption spectra of the dyes with a rhodol core (**4**, **11–14** and **17**) feature an intense band located in the 490–540 nm region (in toluene), and weak features below 400 nm. Corresponding emission spectra cover a narrow spectral region with maxima at ~ 550 nm (in toluene). The absorption solvatochromism of these new rhodols is moderate. Conversely, the vibronic bandshape is largely affected by the solvent polarity, with the contribution from the 0–0 line increasing in polar solvents at the expense of higher replicas. This effect is responsible for a redshift of the λ_{abs}^{max} up to 17200 cm^{-1} for compound **11**, when replacing toluene with DMSO. Emission is also weakly solvatochromic, suggesting that these dyes have similar polarity in the ground and the first excited state. The fluorescence quantum yield (ϕ_{fl}), already large in non-polar solvents, further increases up to more than 0.8 in strongly polar DMSO and acetonitrile solvents. Emission lifetimes, in the 3.5-4 ns range, are marginally affected by the solvent.

The replacement of dialkylamino substituent at position 6 (dye **12**) with secondary amine (dye **11**) is accompanied by a 1430 cm^{-1} hypsochromic shift of the absorption maximum in toluene, related to the different vibronic band structure. The blue-shift reduces to only ~380 cm^{-1} in chloroform, where the two dyes have a similar bandshape (Figure S3). On the other hand, the rigidification of amine substituent (**12**→**4**) induces

Table 2. Spectroscopic properties of target rhodols and merocyanines in different solvents: absorption and emission maxima (λ_{abs}^{max} and λ_{em}^{max}), Stokes shifts, fluorescence quantum yield (ϕ_{fl}) and emission lifetime.

	Solvent	λ_{abs}^{max} /nm	λ_{em}^{max} /nm	Stokes shift /cm^{-1}	ϕ_{fl} [a]	Lifetime /ns
4	Cyclohexane	498	546	1800	0.67	3.93
	Toluene	542	558	500	0.68	3.76
	Chloroform	551	562	350	0.84	3.81
	Acetone	546	567	700	0.85	4.04
	DMSO	554	576	700	0.85	3.70
9	Toluene	528	586	1900	0.21	1.31
	Chloroform	572	596	700	0.72	3.33
	Acetone	566	619	1500	0.71	3.56
	Acetonitrile	566	629	1800	0.52	2.74
10	Toluene	575	598	700	0.51	2.80
	Chloroform	586	625	1100	0.73	3.86
	Acetone	581	655	2000	0.38	2.33
	Acetonitrile	583	667	2200	0.13	–[b]
11	Toluene	491	550	2200	0.43	3.03
	Chloroform	530	546	550	0.75	3.95
	Acetone	527	547	700	0.77	4.08
	DMSO	536	555	600	0.91	3.51
12	Hexane	485	539	2100	0.72	3.46
	Toluene	528	550	750	0.68	3.57
	Chloroform	541	554	400	0.91	3.69
	Acetone	533	557	800	0.89	3.58
	DMSO	542	567	800	0.66	2.58
13	Chloroform	536	550	500	0.91	3.57
	Acetone	533	555	750	0.91	3.73
	Acetonitrile	533	555	750	0.73	3.24
14	Toluene	527	550	800	0.68	3.56
	Chloroform	537	548	400	0.96	3.56
	Acetone	534	552	600	0.90	3.80
	Acetonitrile	534	554	700	0.53	3.62
15	Hexane	519	578	2000	0.10	0.81 (62%); 1.18 (38%)[c]
	Toluene	566	650	2300	0.50	4.69
	Chloroform	584	739	3600	0.10	1.40
	Acetone	575	798	4900	0.01	–[d]
	Acetonitrile	578	–[d]	–[d]	–[d]	–[d]
16	Toluene	527	594	2200	0.52	1.31 (21%); 2.45 (79%)[c]
	Chloroform	545	665	3300	0.44	2.63
	Acetone	545	685	3750	0.34	2.16
	Acetonitrile	547	721	4400	0.08	0.59 (93%); 1.73 (7%)[c]
17	Toluene	531	559	950	0.08	0.47 (73%); 2.83 (27%)[c]
	Chloroform	536	558	700	0.62	2.82
	Acetone	534	563	1000	0.40	1.98
	DMSO	544	571	900	0.62	2.55

[a] Standard: fluorescein in NaOH(aq) 0.1 M. [b] Too short to be estimated (≪ 1 ns). [c] Amplitude in brackets. [d] Weak emission.

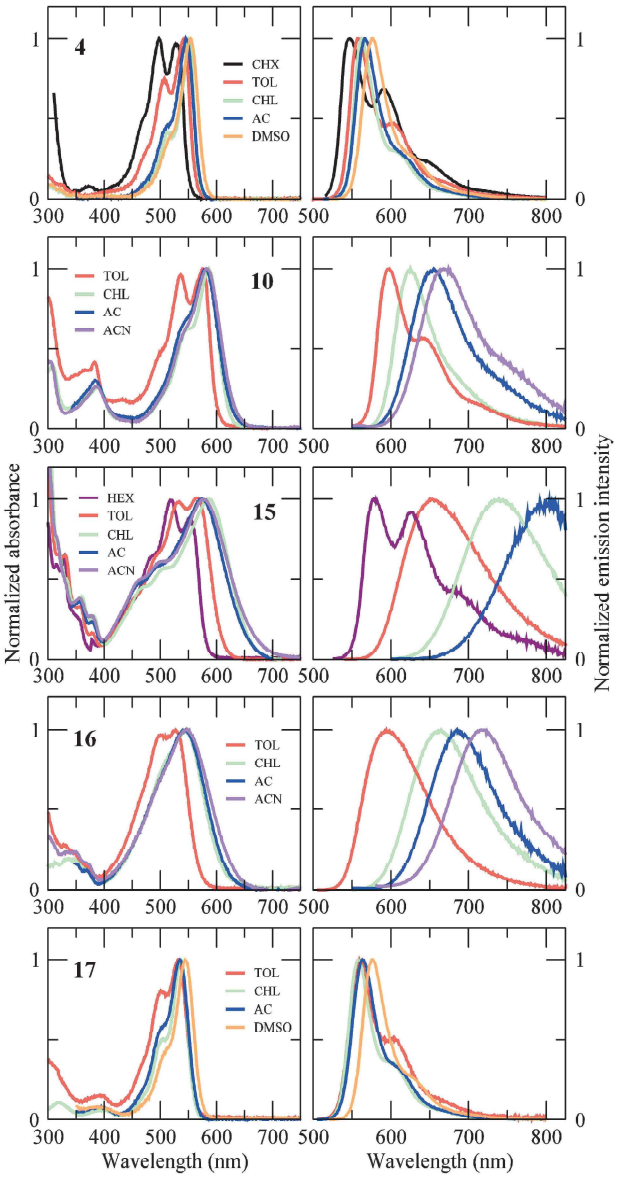

Figure 1. Normalized absorption (left) and emission (right) spectra of compounds **4**, **10**, **15**, **16** and **17** in solvents of different polarity (CHX: cyclohexane, HEX: hexane, TOL: toluene, CHL: chloroform, AC: acetone, ACN: acetonitrile, DMSO: dimethyl sulfoxide).

instead a bathochromic shift. All these changes have minor impact on ϕ_{fl}. The insertion of OH group at position 8 (dyes **13** and **14**) marginally affects the photophysics of rhodols.

The main photophysical properties of the trifluororhodols (intense absorption in the visible, narrow orange emission, marginal effect of solvent polarity) are qualitatively and quantitatively similar to those of rhodol **17**, substituted with ester groups instead of fluorine atoms.[16] However, trifluororhodols **4** and **11–14** have a larger fluorescence quantum yield with respect to **17**.

The π-expansion of rhodol **12** towards angular merocyanine **15** leads to a red-shift and to a sizeable broadening of the absorption band, that covers most of the visible window (400–700 nm in polar solvents). The emission of **15** is bathochromically shifted compared to **12**, and is highly sensitive to solvent polarity: its vibronic structure, well resolved in low-polarity environments (hexane), blurs as the solvent polarity increases. Concomitantly, the emission shifts to the red, with $\lambda_{em}^{max} =$ 578 nm in hexane and ≈800 nm in acetone. Its fluorescence intensity decreases fast in polar solvents, and vanishes in acetonitrile. The different behavior of merocyanine **15** is related to its specific structure that puts it apart from the rhodol family.

Further modification towards fully linear architecture (**15**→**16**) results in a hypsochromic shift of absorption and emission (e.g. 665 nm vs. 739 nm in $CHCl_3$). As for **15**, the absorption spectrum of the linear dye **16** features a broad, almost featureless and marginally solvatochromic band in the visible. Similarly, its fluorescence spectrum is remarkably red-shifted as the solvent polarity is increased (λ_{em}^{max} moves from ~ 600 nm in toluene to > 700 nm in acetonitrile).

Merocyanines **9** and **10** are very interesting. Their absorption resembles that of rhodols **4** and **12**, with analogous influence of rigidification of amine substituent (i.e. a bathochromic shift of both absorption and emission bands, see Figure S3). These dyes show a stronger solvatofluorochromism compared to their rhodol analogues, and their emission red-shifts by approx. 50–70 nm (1200-1700 cm^{-1}) from toluene to CH_3CN. Their fluorescence quantum yields are low in non-polar solvents, reach maximum values (up to 0.7) in solvents of moderate polarity, and drop again to 0.2–0.5 in CH_3CN.

The dependencies of the emission wavenumbers of all the dyes upon two commonly used solvent polarity parameters are shown in Figure S4. In particular, we selected the $f(\varepsilon_{st}) - f(\varepsilon_{opt})$ parameter, to have Lippert–Mataga plots[33,34] (see Equation S4 and successive discussion for the definition of *f*) and Reichardt's $E_T(30)$.[35] Only dyes **10**, **15** and **16** are significantly solvatofluorochromic, with a monotonic and almost linear dependence. The greater slope is shown by dye **15**, followed by **16** and then **10**.

Rhodol-type merocyanines **9** and **10** represent the architectures which were heretofore unknown, whereas a merocyanine possessing essentially the same chromophore as **16** was recently published by Ahn and co-workers.[36] Benzo[*b*]xantene-3-one derivative reported by these authors (**ABXO 1**, Figure S5), in analogy to merocyanine **16**, features a strong absorption band at 540–550 nm, and similar fluorescence quantum yield (10% for **ABXO 1** vs 8% for **16**). Importantly, the lack of fluorine atoms shifts hypsochromically the emission of **ABXO 1** (36 nm in polar media), positioning this dye among deep-red fluorophores, while compound **16** emits in the near infra-red region.

Among other rhodol-type merocyanines or π-expanded rhodols known in the literature, particularly interesting is **BRosol** (Figure S5),[37] vinylogous to rhodole **4** with the conjugation chain extended by a benzene ring. It shows moderate solvatofluorochromism in contrast to dye **4**, however the direct comparison is not possible as spectra were measured in different solvents. Nonetheless, a pronounced difference can be clearly observed in the emission intensity, with fluorescence

quantum yield reaching 27% in DCM for **BRosol** vs ca. 85% in chloroform, acetone and DMSO for **4**, favoring the latter dye in bioimaging applications.

Benzo[*c*]xanthene-based seminaphthorhodafluor (**SNARF 1**, Figure S5) reported by the Strongin's group,[38] possesses an angular structure similar to the one in dye **15**. Even though there is no sufficient fluorescence data for these emitters, comparison of the fluorescence spectra reveals significant influence of the substitution pattern and nature of substituents on the emission maxima. Whilst a tiny Stokes shift is observed for **SNARF 1** in polar media, merocyanine **15** is characterized by significant red-shift of the fluorescence band (located at ca. 800 nm in acetone), with a Stokes shift up to 4800 cm^{-1}.

On the other hand, reported by the same group, regioisomeric benzo[*c*]xanthene-based **SNARFs 2** (Figure S5)[39] possesses π-expanded core from the electron-acceptor side of the dye. Even though such modification did not result in a striking bathochromic shift of the absorption maxima (up to 556 nm in MeOH), the emission of **SNARFs 2** appeared in the red part of the spectrum (up to 630 nm) with maximum efficiency on ~20% (in MeOH), which is however less favorable compared to the optical properties of **15** in terms of future applications.

The photochemical stability of some representative compounds (trifluororhodol **4**, non-fluorinated rhodol **17**, merocyanines **10**, **15** and **16**) was investigated in chloroform solution. Photodecomposition quantum yields[40] were estimated adopting the method proposed by Belfield et al.,[41] based on the time-dependent variation of the optical density of a solution irradiated with a continuous light source (details in the Supporting Information and Figure S5). The photodecomposition quantum yield, ϕ_D, estimated for the trifluororhodol **4** (5×10^{-6}) is one order of magnitude lower than for the non-fluorinated analogue **17** (3×10^{-5}), indicating a positive effect of the new substitution pattern on photochemical stability. Compared to **4**, the two π-expanded rhodols **15** and **16** are more susceptible to photodecomposition, with the linear dye (**16**) being considerably less stable ($\phi_D = 7\times10^{-5}$) than the angular one (**15**, $\phi_D = 9\times10^{-6}$). Hybrid coumarino-rhodol **10**, instead, shows an excellent photochemical stability, with the smallest ϕ_D among all compounds ($\phi_D = 8\times10^{-7}$). Overall, the new dyes have ϕ_D comparable to literature values for fluorescein (2×10^{-5}–1×10^{-4}) and rhodamine 6G (1×10^{-6}–2×10^{-5}).[40]

The two-photon absorption (2PA) spectra of selected dyes (Figure 2 and S7) were collected in chloroform, exploiting the 2PEF technique.[42–44] The low symmetry of the dyes makes all electronic transitions allowed both in one-photon absorption (1PA) and 2PA processes.

In the experimentally accessible window (700–1300 nm), two bands dominate the 2PA spectrum of rhodols **4** and **17**. The lowest-energy band peaks around 1000 nm (photon energy) and matches the main 1PA band. However, the vibronic bandshape of the 1PA and 2PA bands are remarkably different: for both dyes, the most intense feature in the 1PA spectrum is due to the 0–0 transition, while in 2PA the most intense peak is related to the 0–1 transition, with a consequent apparent blue shift of the 2PA vs the 1PA band. The origin of this interesting feature will be discussed later on. A second featureless 2PA band occurs around 800 nm, in correspondence with a very weak 1PA feature. The 2PA cross-section amounts to $\sigma_2 \approx 40$ GM for the low-energy band of both dyes and reaches 40 GM and 120 GM for the higher energy 2PA band of **4** and **17**, respectively. These values are in line with available data for rhodols.[45]

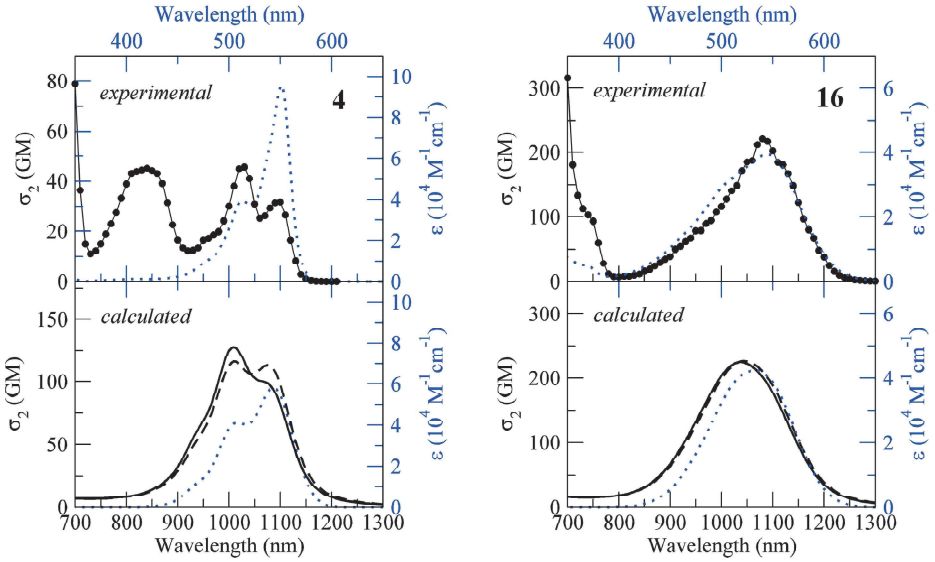

Figure 2. Top panels: experimental two-photon absorption cross-section σ_2 (black circles) and molar extinction coefficient ε (blue dotted line) of **4** and **16** collected in chloroform solution. Experimental uncertainties on σ_2 are ~10% for **4** and 20–25% for **16**. Bottom panels: 2PA (black) and 1PA (blue) spectra calculated in the essential-state model ($\varepsilon_{or} = 0.25$ eV for **4** and 0.38 eV for **16**). Calculated 2PA spectra shown as continuous lines refer to the full calculation, while 2PA spectra shown as dashed lines refer to spectra calculated without accounting for the vibrational channel. 1 GM = 10^{-50} cm^4 s photons^{-1}.

The 2PA spectrum of dye **10** has some qualitative analogies with that of rhodols: the lowest-energy 2PA band, corresponding to the main 1PA peak, has a resolved vibronic structure with an apparent blue shift vs 1PA due the different vibronic structure. However, the cross-section of **10** at the band maximum ($\sigma_2 \approx 150$ GM) is more than three times larger than for rhodols **4** and **17**. An additional 2PA band at higher energy, with slightly higher similar cross-section, presents two maxima at 800 and 870 nm corresponding to two weak 1PA features. Merocyanines **15** and **16**, instead, show a qualitatively different behavior (Figure 2). Their 2PA spectra show a broad band mimicking the shape of the corresponding 1PA spectra, with cross-sections up to 150–200 GM.

Excitation anisotropy of **4**, **10**, **15**, **16** and **17** (Figure S8) was collected in 2-methyltetrahydrofuran solution undercooled at 77 K to yield a transparent glass. At this temperature, the rotational motion of the dyes is frozen, so that the measured anisotropy value corresponds to the fundamental anisotropy r_0. This quantity is related to the angle α between excitation and emission dipole moments:[46,47]

$$r_0 = \frac{2}{5}\left(\frac{3\cos^2\alpha - 1}{2}\right) \quad (1)$$

Since, according to Kasha's rule, emission occurs from the (relaxed) lowest-energy excited state (S_1), r_0 gives information about the angle formed by transition dipole moments of the Kasha state and of the state reached upon absorption at each excitation wavelength, facilitating the individuation of the different electronic states contributing to the absorption spectrum.

For rhodols **4** and **17**, the flat anisotropy over the whole region of the main 1PA band confirms that only one state (S_1) is responsible for the absorption in that spectral region. The dip around 400 nm, in the same region of a weak 1PA signal and of the second 2PA band, suggests the presence of an excited state with different polarization ($\alpha \approx 50^\circ$ or an angle with the same squared cosine), responsible for both linear and nonlinear absorption. At shorter wavelengths ($\lambda < 400$ nm), instead, the behavior of the two dyes is different: the anisotropy of **4** amounts to 0.2 while that of **17** is lower (0.05–0.1), suggesting a different excited-state scenario for the two compounds. The analogy between the low-energy spectral features of **4** and **17** suggests a similar nature of the $S_0 \rightarrow S_1$ transition, irrespective of the different substituents. Therefore, this transition can be associated to the rhodol's merocyanine chromophore, while substitution mainly affects higher-energy states.

The anisotropy of dye **10** is high (~0.3) and constant over the 450–600 nm range, supporting the attribution of its intense absorption band to the $S_0 \rightarrow S_1$ excitation. Moreover, r_0 shows two negative minima (≈ -0.1) at 430 nm and below 390 nm, separated by a local maximum at 415 nm (≈ 0.1), suggesting the presence of several excited states in this spectral region.

Excitation anisotropies of **15** and **16** offer information on the origin of the broad absorption features, and reveals a major difference between the two. For **16**, the anisotropy suggests that the band in the 400–600 nm window is due to a single excited state, S_1, ($r_0 \approx 0.3$ over all this wavelength range), while the second bright excited state is much higher in energy, and is spotted by a dip at $\lambda < 400$ nm ($r_0 \approx 0$–0.05). Conversely, the main absorption band of **15** originates from the contribution of at least two excited states, peaking around 600 and 500 nm respectively, which are revealed by a different anisotropy value (0.3 and 0.05).

Computational results

TDDFT results in gas phase

Additional insight into the electronic structure of the dyes was gathered from a computational investigation utilizing density functional theory (DFT) and its time-dependent extension (TDDFT).[48–51] The ground-state geometry of the two rhodols **4** and **17**, and compounds **10**, **15** and **16** was optimized in the gas phase at the M06-2X/6-31G(d) level of theory,[52] as implemented in the Gaussian16 package.[53] In the computations, the long alkyl chains of **15** have been replaced by ethyl groups, with negligible effect on the electronic properties.

In all dyes, the π-conjugated backbone is almost planar. In dye **17**, the aryl substituent in position 9 is nearly orthogonal to the molecular plane (dihedral angle $\approx 77^\circ$), suggesting a poor conjugation with the rhodol skeleton.[54]

Rhodols, as well as the other expanded dyes presented in this work, belong to the large family of merocyanine dyes. Merocyanines are characterized by a donor and an acceptor group connected by a π-conjugated bridge. Their low-energy photophysics is dominated by two limiting resonance structures: a neutral form and a zwitterionic form, in which one electron is transferred from the amino to the carbonyl group (Figure S9).[17] The length of the two bonds of the conjugated bridge, b_1 and b_2 (Figure S9) can be viewed as an indicator of the weight of the two forms in the ground state. Bond lengths calculated for the target dyes (Table S13) indicate an intermediate character between a single and a double bond, as expected for a conjugated system. In more detail, the small difference between the two bonds points to a slight dominance of the neutral form over the zwitterionic form. Interestingly, the bond-length difference calculated for merocyanine **10** is similar to that of rhodols **4** and **17**, while the difference estimated for **15** and **16** is larger, indicating a smaller mixing between the two limiting structures.

To address excitations, we performed gas phase TDDFT calculations at the M06-2X/6-31G(d) level, on the ground-state optimized geometry. Table 3 summarizes the main results for the three lowest-energy transitions of the dyes. Frontier molecular orbitals (FMOs) involved in the optically-allowed transitions are shown in Figure 3.

For all the dyes, the $S_0 \rightarrow S_1$ is the most intense transition, and corresponds to an almost pure HOMO→LUMO excitation. For rhodols **4** and **17**, as well as for the π-expanded dye **16**, this transition is predicted at similar energy (≈3.1 eV), while it is slightly red-shifted (up to 0.15 eV) for **15** and **10**, in agreement with the experimental trend. The main component of the

Table 3. TDDFT data on selected dyes in the gas phase calculated at M06-2X/6-31G(d) level of theory: transition energy and wavelength λ, oscillator strength *f*, FMO contribution (> 25 %).

	Transition	Energy/eV	λ/nm	*f*	Type [%]
4	$S_0 \rightarrow S_1$	3.09	401	0.750	H→L (94 %)
	$S_0 \rightarrow S_2$	3.67	338	0.000	H-3→L (71 %)
	$S_0 \rightarrow S_3$	3.73	332	0.077	H-1→L (86 %)
10	$S_0 \rightarrow S_1$	2.94	421	0.771	H→L (92 %)
	$S_0 \rightarrow S_2$	3.67	338	0.000	H-4→L (64 %)
	$S_0 \rightarrow S_3$	3.74	331	0.145	H-1→L (69 %)
15	$S_0 \rightarrow S_1$	3.03	409	0.486	H→L (90 %)
	$S_0 \rightarrow S_2$	3.44	360	0.109	H-1→L (82 %)
	$S_0 \rightarrow S_3$	3.60	344	0.000	H-4→L (72 %)
16	$S_0 \rightarrow S_1$	3.12	397	1.022	H→L (93 %)
	$S_0 \rightarrow S_2$	3.22	385	0.006	H-1→L (89 %)
	$S_0 \rightarrow S_3$	3.56	348	0.000	H-4→L (75 %)
17	$S_0 \rightarrow S_1$	3.08	402	0.751	H→L (96 %)
	$S_0 \rightarrow S_2$	3.36	369	0.000	H-2→L (73 %)
	$S_0 \rightarrow S_3$	3.92	316	0.147	H-1→L (85 %)

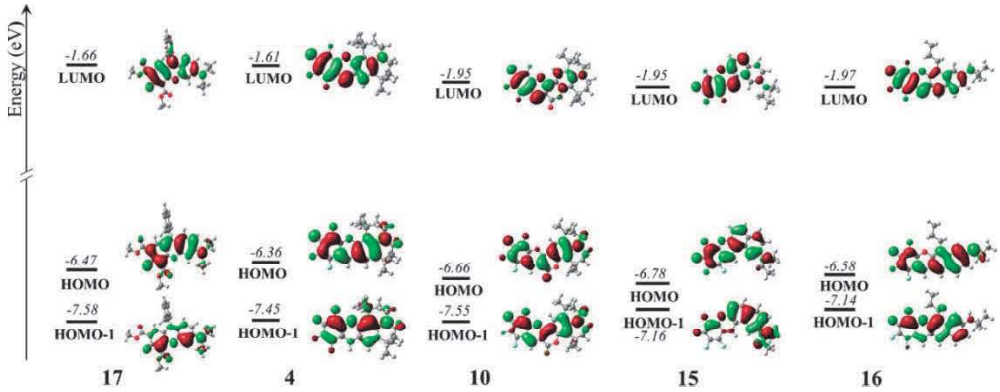

Figure 3. Frontier molecular orbitals (FMOs) of **4**, **10** and **15–17** (DFT M06-2X/6-31G(d) in gas phase; isovalue: 0.02).

associated transition dipole moment is aligned along the axis connecting the amino and the carbonyl groups.

To better understand the variation of the charge distribution upon photoexcitation, we arbitrarily partitioned the target molecules into two moieties (see Figure S10) and compared the cumulative Hirshfeld charges[55] calculated in the two moieties in the ground state and in the S_1 (vertical) state (data in Table S14). In the ground state, a small negative charge resides on the region containing the electron-withdrawing carbonyl group, while charge depletion is observed on the amino group, behaving as an electron donor. Upon photoexcitation to S_1, the charge separation increases in the same direction, confirming the charge-transfer character of the transition.

Moving to higher energies, for dyes **4**, **10** and **17**, the $S_0 \rightarrow S_2$ transition has a $n \rightarrow \pi^*$ character and is dark, while the $S_0 \rightarrow S_3$, mainly a HOMO-1→LUMO excitation, is optically-allowed but its oscillator strength is almost one order of magnitude smaller compared to that of the $S_0 \rightarrow S_1$. The energy difference between $S_0 \rightarrow S_1$ and $S_0 \rightarrow S_3$ amounts to ≈0.8 eV for **10** and **17** and ≈0.6 eV for **4**, in good agreement with the experimental energy gap between the main absorption transition and the lowest-energy weak absorption feature corresponding to an anisotropy dip and to the secondary 2PA band.

The $S_0 \rightarrow S_1$ and $S_0 \rightarrow S_2$ transitions of the expanded merocyanine **15** are closer in energy (0.4 eV), with a comparable oscillator strength, in agreement with the peculiar broad absorption band made up by the contribution of two states, as revealed by anisotropy analysis. Unlike parent rhodols, whose FMOs extend over both amino and carbonyl groups suggesting strong conjugation, the HOMO-1 and LUMO of dye **15** are localized on the moieties containing the amino group (donor) and the carbonyl group (acceptor), respectively, indicating a stronger charge-transfer character of the $S_0 \rightarrow S_2$ transition, as confirmed by the large increase of charge separation (Table S14).

For the linear merocyanine **16**, instead, absorption is dominated by the $S_0 \rightarrow S_1$ transition, with charge-transfer nature.

Computational results in solution

Solvation effects usually play an important role in the spectroscopy of polar and polarizable solutes like merocyanines. Thus, the proper description of the interaction with the solvent is crucial to understand solvatochromism and rationalize the different behavior of the dyes.

To address solvation, we adopt a method recently proposed[56,57] to properly account for the different timescales of the two main solvation components. On one side, electronic solvation, related to the electronic degrees of freedom of the solvent, is very fast and will be dealt with in the antiadiabatic approximation. On the other side, polar solvation, related to the orientational motion of polar solvent molecules, is very slow and will be dealt with in the adiabatic approximation. The approach proposed in Ref.,[57] is shortly summarized in Supporting Information.

Main results obtained for rhodol **4** and merocyanine **16** are presented in Figure 4, and describe the evolution with the solvent polarity of the transition energies and dipole moments for the three lowest-energy transitions (top and bottom panels, respectively) as well as the permanent dipole moments in the ground state and in the three lowest-energy electronic excited states (middle panels). Analogous figures for **10**, **15** and **17** are provided in Supporting Information (Figures S11–S13).

The permanent dipole moment of **4** in the ground state is large (13–15 Debye) and is marginally affected by the solvent polarity. Upon vertical excitation to S_1, the dipole moment shows a moderate increase to 20–23 Debye, explaining the observation of a small absorption solvatochromism. Conversely, in the relaxed S_1 geometry, S_0 and S_1 have similar polarity (15–20 Debye) in all the investigated solvents, pointing to a negligible solvatochromic effect. Indeed, calculated emission energies (2.5–2.6 eV) are barely affected by the solvent polarity, in very good agreement with experimental data. Quantitatively similar results were obtained for rhodol **17** (Figure S13), in line with the similar photophysics of the two dyes.

Dye **16** also has a large permanent dipole moment in the ground state (15–20 Debye) but, at variance with **4** and **17**, the permanent dipole moment of its S_1 state is even larger, amounting to ≈35 Debye. This large variation of the dipole moment upon excitation justifies the pronounced positive emission solvatochromism of merocyanine **16**. The calculated shift from toluene to acetonitrile of ≈0.5 eV compares well with the experimental one (≈0.4 eV). Concerning absorption, S_1 and S_2 states, closely spaced in the gas phase, are separated by a wide energy gap in solution (>0.9 eV), improving the agreement with experimental data.

The hybrid coumarino-merocyanine **10** (Figure S11) has an intermediate behavior between **4** and **16**: its permanent dipole moment shows a moderate increase upon excitation, from 13–15 Debye in the ground state to 25–30 Debye in S_1, pointing to a more pronounced solvatofluorochromism compared to rhodols.

Fairly accurate results are also obtained for dye **15**, notwithstanding its complex electronic structure with two nearby electronic states (Figure S12). In solution, even in nonpolar solvents, the state with the largest charge-transfer character is stabilized: the S_1 state is characterized by a sizable dipole moment (25–35 Debye), while S_2 has a similar polarity as the ground state. Accordingly, in absorption the $S_0 \rightarrow S_1$ transition moves slightly to the red with increasing solvent

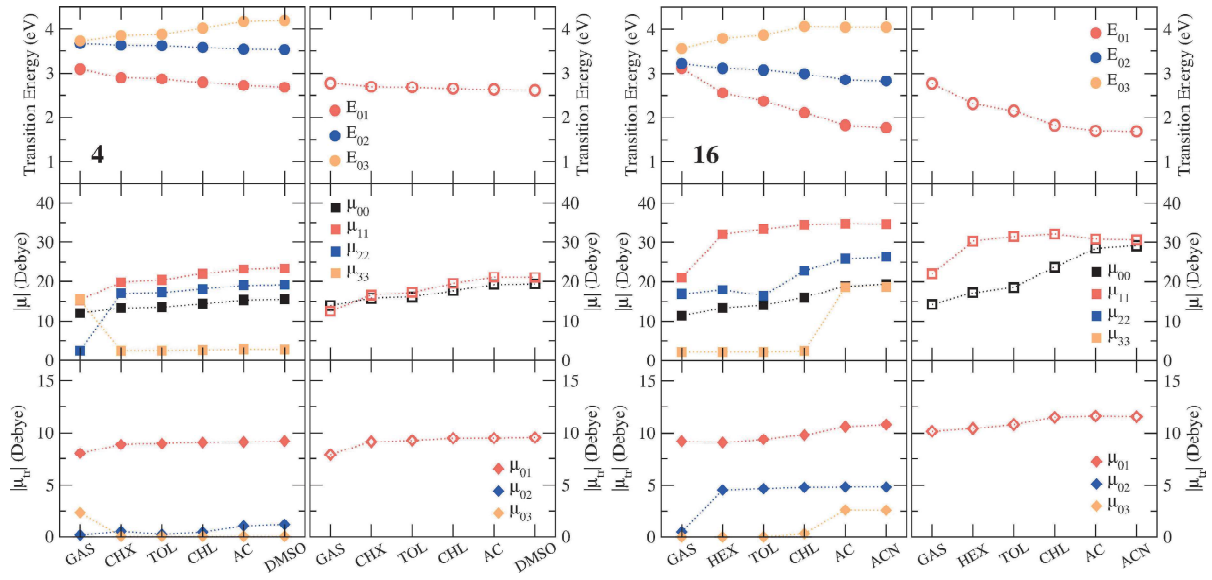

Figure 4. Properties of dyes **4** and **16** calculated in gas phase and in different solvents adopting the antiadiabatic approximation for electronic solvation and the adiabatic approximation for orientational solvation: transition energies E_{ij} (top panels), permanent dipole moments μ_{ii} (middle panels) and transition dipole moments μ_{ij} (bottom panels). HEX: hexane, CHX: cyclohexane, TOL: toluene, CHL: chloroform, AC: acetone, ACN: acetonitrile, DMSO: dimethyl sulfoxide, GAS: gas phase. Solid symbols are relevant to the absorption process, empty symbols to the emission process. Properties were calculated at the equilibrium value of the orientational component of the reaction field (F_{or}, see Supporting Information for the state of interest (S_0 for absorption and S_1 for emission).

polarity, while $S_0 \rightarrow S_2$ remains unshifted, mimicking the experimental red-shift and widening of the band. As for **16**, the large increase of permanent dipole moment upon excitation also in the relaxed geometry leads to a sizeable emission solvatochromism.

Essential-state model

TDDFT analysis points to a fairly complex electronic structure of the target dyes. Nevertheless, their photophysics is dominated by the lowest-energy transition, with a clear charge-transfer character. This invites to adopt a simple two-state model, extensively applied to describe the spectral properties of push-pull chromophores.[58–60] Specifically, we focused on dyes **4** and **16**, that show distinctively different behavior.

We describe the two compounds as conjugated donor-acceptor $D-\pi-A$ dyes, resonating between two limiting structures, a neutral form ($D-\pi-A$) and a zwitterionic form ($D^{+}-\pi-A^{-}$), and we chose these two structures as the electronic basis states for the molecular Hamiltonian. The two states are mixed in a ground state with permanent dipole $\mu_0\rho$, where μ_0 is the dipole moment of the zwitterionic state, and ρ, also called ionicity, is its weight in the ground state. This minimal model for the electronic structure is extended to account for vibrational coupling and polar solvation (see Supporting Information for further details) and allows for a detailed description of spectral band-shapes and their dependence on the solvent polarity.[61,62]

Calculated absorption and emission spectra (Figure 5) provide a good description of the lowest-lying transition and reproduce the solvatochromic shifts as well as the evolution of the spectral bandshape with solvent polarity.

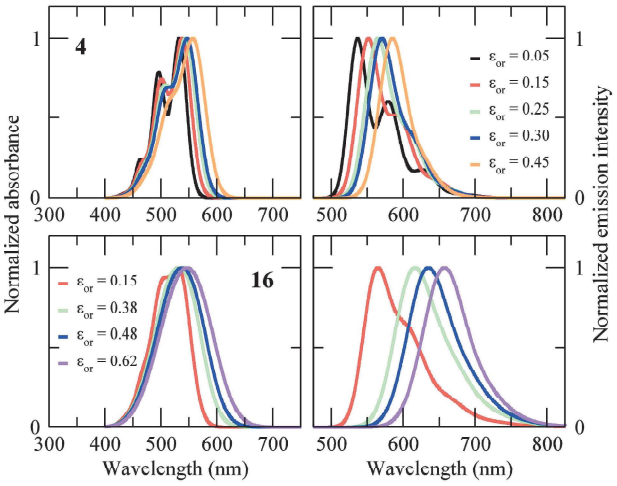

Figure 5. Normalized absorption (left) and emission (right) spectra of dyes **4** and **16** simulated with the two-state model in different solvents (different ε_{or} values, see legend). Model parameters for **4**: $z_0 = 0.80$ eV, $\sqrt{2}t = -1.00$ eV, $\mu_0 = 20.5$ D, $\omega_v = 0.20$ eV, $\omega_t = 0.10$ eV, $\varepsilon_v = 0.625$ eV. Model parameters for **16**: $z_0 = 0.94$ eV, $\sqrt{2}t = -0.86$ eV, $\mu_0 = 23.5$ D, $\omega_v = 0.18$ eV, $\omega_t = 0.14$ eV, $\varepsilon_v = 0.286$ eV. The spectral bandwidth γ (half-width at half-maximum) assigned to each vibronic transition was set to 0.06 eV. ε_{or} values mimicking different solvents are reported in eV.

The estimated ground-state ionicity ρ of **4** at equilibrium goes from 0.21 in cyclohexane to 0.24 in dimethyl sulfoxide, while the ionicity of **16** stays almost constant at 0.15–0.16 in all solvents. This finding indicates that the charge separation in the ground state is lower for the π-expanded dye, in agreement with TDDFT results, and implies a larger polarity increase in the excited state, in line with a stronger solvatofluorochromism.

Within this model, only the lowest-energy electronic transition can be addressed, but the relevant 2PA spectrum can be calculated fully accounting for the vibronic bandshape. In all investigated molecules, the lack of symmetry makes the lowest excited state allowed both in 1PA and 2PA. In spite of that, for rhodol **4** the linear and the nonlinear absorption spectra show a distinctively different shape, with the 0–0 vibronic line dominating the 1PA spectrum and the 0–1 vibronic line dominating 2PA. This result is well reproduced in the calculated spectra (Figure 2, bottom panels), fully in line with the behavior predicted more than 20 years back for dyes with sizable ρ.[63] It is interesting to notice in this context the sizable contributions of the "vibrational channels" to 2PA spectra, i.e. of the terms in the sum-over-state expression (Eq. S9) involving the vibrational states in the electronic ground state manifold. Conversely, the 2PA spectrum of **16** lacks a vibronic structure and the shape of the 2PA band is more similar to the 1PA bandshape, as expected for a dye with a comparatively small ρ,[63] in good agreement with experiment.

Conclusions

A novel synthetic approach towards rhodols and rhodol-type merocyanines was developed. The reactivity of the formyl group in tetrafluorohydroxybenzaldehyde proved to be strong enough to induce the Friedel–Crafts reaction with 3-dialkylaminophenol without an external acidic catalyst. The subsequent nucleophilic aromatic substitution leads to the formation of a merocyanine chromophore in an overall one-pot process. This new synthetic strategy leads to heretofore inaccessible rhodols lacking a substituent at position 9 and having three fluorine atoms on the electron-accepting ring. We have proven that also hydroxy-amino-coumarins as well as aminonaphthalenols undergo this tandem reaction with 4-hydroxy-2,3,5,6-tetrafluorobenzaldehyde, giving rise to heretofore unknown classes of fluorophores.

A comprehensive photophysical characterization has shown that, in rhodols, the presence of three fluorine atoms marginally affects the degree of charge transfer and the sensitivity to the environment compared to other electron-withdrawing substituents like ester groups. However, the new substitution pattern allows to increase the brightness (up to 80,000 M^{-1} cm^{-1}) and achieve an excellent photochemical stability even though position 9 is free.

The π-expansion of the rhodol-type core in a linear or angular fashion has a significant impact on the photophysical properties: not only it allows to shift absorption and emission

across the visible window, but it also introduces a large emission solvatochromism, that is not seen in rhodols. A remarkable exception are hybrid coumarino-merocyanine that, in spite of a more complex π-conjugated architecture, basically retain a rhodol-like behavior.

Our computational investigation supported the description of the new fluorophores as merocyanine dyes. Indeed, the lowest absorption band has a charge-transfer character, suggesting that the ground and the first excited state can be described as resonating between a neutral and a charge-separated (zwitterionic) structure.

In rhodols, the contribution of the charge-separated state in the ground state is large, leading to sizeable permanent dipole moments. Upon excitation, the permanent dipole moment only slightly increases, explaining their weak solvatochromism and locating rhodols rather close to the cyanine limit. The progressive substantial loss of intensity of vibronic replicas (both in absorption and emission spectra) for increasing solvent polarity is similarly in line with a cyanine-like electronic structure. Conversely, π-expanded systems are characterized by a more neutral ground state, and a sizeable increase of permanent dipole moment upon charge-transfer occurs. Their highly polar S_1 state is stabilized in polar solvents, yielding large emission solvatochromic shifts.

Another interesting difference between the investigated dyes concerns 2PA. All dyes are noncentrosymmetric, so that the $S_0 \rightarrow S_1$ transition is symmetry-allowed both 1PA and 2PA. However, while for π-expanded dyes 1PA and 2PA bands are featureless and almost superimposable, for rhodol and rhodol-like systems the 2PA band, characterized by a prominent vibronic structure, is distorted with respect to the 1PA band, and the rescaled 2PA maximum is blue-shifted compared to the 1PA maximum.

The charge-transfer nature of the first electronic transition supported the description of the two representative rhodols through a minimal model only accounting for two basis states, corresponding to the limiting resonance forms. In this model electron-phonon coupling and inhomogeneous broadening effects from polar solvation can be investigated, addressing quantitatively the bandshape of linear and nonlinear spectra. Along these lines, we were able to rationalize the observed blue-shift and different band-shape of 2PA vs 1PA of rhodols as due to a significant contribution of the "vibrational channel".[63] This finding further confirms that rhodols are not too far from the cyanine limit.

The moderate 2PA response of trifluororhodols and rhodol-like systems in the near-IR region, combined with orange-red emission, high fluorescence quantum yields (also in high polarity environments) and good photostability, make them suitable for application as fluorescent imaging probes in two-photon microscopy.

The reported new synthetic procedures offer new possibilities for fine-tuning the properties of an interesting and widespread class of fluorophores, a result of paramount importance particularly in view of their multifarious applications.

Acknowledgements

The authors thank the Foundation for Polish Science (TEAM POIR.04.04.00-00-3CF4/16-00) and the European Union Horizon 2020 research and innovation programme (GA 101007804, Micro4Nano). Work at UNIPR also received financial support from PNRR-MUR project ECS_00000033_ECOSISTER and benefited from the HPC (High Performance Computing) facility of the University of Parma and from the equipment and framework of the COMP-HUB and COMP–R Initiatives, funded by the 'Departments of Excellence' program of the Italian Ministry for University and Research (MIUR, 2018–2022 and MUR, 2023–2027). We thank Mr. Joseph Milton for amending the manuscript.

Conflict of Interests

The authors declare no conflict of interest.

Data Availability Statement

The data that support the findings of this study are available from the corresponding author upon reasonable request.

Keywords: dyes/pigments · fluorescent probes · intramolecular charge transfer · linear and nonlinear optical spectroscopy · theoretical modelling

[1] I. Johnson, M. T. Z. Spence, Eds., *Molecular Probes Handbook, A Guide to Fluorescent Probes and Labeling Technologies*, Life Technologies Corporation, **2010**.
[2] P. Shieh, V. T. Dien, B. J. Beahm, J. M. Castellano, T. Wyss-Coray, C. R. Bertozzi, *J. Am. Chem. Soc.* **2015**, *137*, 7145–7151.
[3] G. Lukinavičius, L. Reymond, K. Umezawa, O. Sallin, E. D'Este, F. Göttfert, H. Ta, S. W. Hell, Y. Urano, K. Johnsson, *J. Am. Chem. Soc.* **2016**, *138*, 9365–9368.
[4] T. Ikeno, T. Nagano, K. Hanaoka, *Chem. Asian J.* **2017**, *12*, 1435–1446.
[5] M. Grzybowski, M. Taki, S. Yamaguchi, *Chem. A Eur. J.* **2017**, *23*, 13028–13032.
[6] M. Grzybowski, M. Taki, K. Kajiwara, S. Yamaguchi, *Chem. Eur. J.* **2020**, *26*, 7912–7917.
[7] J. Liu, Y. Q. Sun, H. Zhang, H. Shi, Y. Shi, W. Guo, *ACS Appl. Mater. Interfaces* **2016**, *8*, 22953–22962.
[8] A. N. Butkevich, G. Y. Mitronova, S. C. Sidenstein, J. L. Klocke, D. Kamin, D. N. H. Meineke, E. D'Este, P. T. Kraemer, J. G. Danzl, V. N. Belov, et al., *Angew. Chem. Int. Ed.* **2016**, *55*, 3290–3294.
[9] J. B. Grimm, A. J. Sung, W. R. Legant, P. Hulamm, S. M. Matlosz, E. Betzig, L. D. Lavis, *ACS Chem. Biol.* **2013**, *8*, 1303–1310.
[10] M. V. Sednev, C. A. Wurm, V. N. Belov, S. W. Hell, *Bioconjugate Chem.* **2013**, *24*, 690–700.
[11] S. Takahashi, Y. Kagami, K. Hanaoka, T. Terai, T. Komatsu, T. Ueno, M. Uchiyama, I. Koyama-Honda, N. Mizushima, T. Taguchi, et al., *J. Am. Chem. Soc.* **2018**, *140*, 5925–5933.
[12] L. D. Lavis, *Biochemistry* **2017**, *56*, 5165–5170.
[13] Y. J. Gong, X. B. Zhang, G. J. Mao, L. Su, H. M. Meng, W. Tan, S. Feng, G. Zhang, *Chem. Sci.* **2016**, *7*, 2275–2285.
[14] J. Chan, S. C. Dodani, C. J. Chang, *Nat. Chem.* **2012**, *4*, 973–984.
[15] C. Deo, S. H. Sheu, J. Seo, D. E. Clapham, L. D. Lavis, *J. Am. Chem. Soc.* **2019**, *141*, 13734–13738.
[16] P. Shieh, M. J. Hangauer, C. R. Bertozzi, *J. Am. Chem. Soc.* **2012**, *134*, 17428–17431.

[17] Y. M. Poronik, K. V. Vygranenko, D. Gryko, D. T. Gryko, *Chem. Soc. Rev.* **2019**, *48*, 5242–5265.
[18] M. Grzybowski, O. Morawski, K. Nowak, P. Garbacz, *Chem. Commun.* **2022**, *58*, 5455–5458.
[19] W. C. Sun, K. R. Gee, D. H. Klaubert, R. P. Haugland, *J. Org. Chem.* **1997**, *62*, 6469–6475.
[20] K. V. Vygranenko, Y. M. Poronik, M. H. E. Bousquet, O. Vakuliuk, D. Jacquemin, D. T. Gryko, *Chem. Commun.* **2022**, *58*, 1542–1545.
[21] D. T. Gryko, D. Wyrostek, A. Nowak-Król, K. Abramczyk, M. K. Rogacki, *Synthesis* **2008**, 4028–4032.
[22] Q. He, E. W. Miller, A. P. Wong, C. J. Chang, *J. Am. Chem. Soc.* **2006**, *128*, 9316–9317.
[23] A. C. Benniston, D. B. Rewinska, *Org. Biomol. Chem.* **2006**, *4*, 3886–3888.
[24] R. Bandichhor, A. D. Petrescu, A. Vespa, A. B. Kier, F. Schroeder, K. Burgess, *Bioconjugate Chem.* **2006**, *17*, 1219–1225.
[25] J. C. Duff, E. J. Bills, *J. Chem. Soc.* **1932**, 1987.
[26] W. E. Smith, *J. Org. Chem.* **1972**, *37*, 3972.
[27] K. Skonieczny, G. Charalambidis, M. Tasior, M. Krzeszewski, A. Kalkan-Burat, A. G. Coutsolelos, D. T. Gryko, *Synthesis* **2012**, *44*, 3683–3687.
[28] G. R. Geier, Y. Ciringh, F. Li, D. M. Haynes, J. S. Lindsey, *Org. Lett.* **2000**, *2*, 1745–1748.
[29] S. Kobayashi, *Eur. J. Org. Chem.* **1999**, 15–27.
[30] X. Wang, Y. Wang, D.-M. Du, J. Xu, *J. Mol. Catal. A* **2006**, *255*, 31–35.
[31] Y. Terazono, E. J. North, A. L. Moore, T. A. Moore, D. Gust, *Org. Lett.* **2012**, *14*, 1776–1779.
[32] J.-J.– Zhang, M.-C. Tang, Y. Fu, K.-H. Low, J. Ma, L. Yang, J. J. Weigand, J. Liu, V. W.-W. Yam, X. Feng, *Angew. Chem. Int. Ed.* **2020**, *60*, 2833–2838.
[33] E. Lippert, *Z. Für Nat. A.* **1955**, *10*, 541–545.
[34] N. Mataga, Y. Kaifu, M. Koizumi, *Bull. Chem. Soc. Jpn.* **1955**, *28*, 690–691.
[35] C. Reichardt, *Chem. Rev.* **1994**, *94*, 2319–2358.
[36] U. Tamima, C. W. Song, M. Santra, Y. J. Reo, H. Banna, M. R. Islam, K. H. Ahn, *Sens. Actuators B* **2020**, *322*, 128588.
[37] M. Dai, Y. J. Reo, C. W. Song, Y. J. Yang, K. H. Ahn, *Chem. Sci.* **2020**, *11*, 8901–8911.
[38] L. Wang, C. W. Barth, M. Sibrian-Vazquez, J. O. Escobedo, M. Lowry, J. Muschler, H. Li, S. L. Gibbs, R. M. Strongin, *ACS Omega* **2017**, *2*, 154–163.
[39] L. G. Wang, I. Munhenzva, M. Sibrian-Vazquez, J. O. Escobedo, C. H. Kitts, F. R. Fronczek, R. M. Strongin, *J. Org. Chem.* **2019**, *84*, 2585–2595.
[40] C. Eggeling, J. Widengren, R. Rigler, C. A. M. Seidel, in *Appl. Fluoresc. Chem. Biol. Med.* (Eds.: W. Rettig, B. Strehmel, M. Schrader, H. Seifert), Springer-Verlag, Berlin Heidelberg, **1999**, pp. 193–240.
[41] K. D. Belfield, M. V. Bondar, Y. Liu, O. V. Przhonska, *J. Phys. Org. Chem.* **2003**, *16*, 69–78.
[42] C. Xu, W. W. Webb, *J. Opt. Soc. Am. B* **1996**, *13*, 481.
[43] F. Terenziani, C. Katan, E. Badaeva, S. Tretiak, M. Blanchard-Desce, *Adv. Mater.* **2008**, *20*, 4641–4678.
[44] M. A. Albota, C. Xu, W. W. Webb, *Appl. Opt.* **1998**, *37*, 7352.
[45] Y. M. Poronik, G. Clermont, M. Blanchard-Desce, D. T. Gryko, *J. Org. Chem.* **2013**, *78*, 11721–11732.
[46] J. R. Lakowicz, *Principles of Fluorescence Spectroscopy*, Springer, New York, USA, **2006**.
[47] B. Valeur, *Molecular Fluorescence. Principles and Applications*, Wiley-VCH Verlag GmbH, **2001**.
[48] E. Runge, E. K. U. Gross, *Phys. Rev. Lett.* **1984**, *52*, 997–1000.
[49] R. Bauernschmitt, R. Ahlrichs, *Chem. Phys. Lett.* **1996**, *256*, 454–464.
[50] M. E. Casida, C. Jamorski, K. C. Casida, D. R. Salahub, *J. Chem. Phys.* **1998**, *108*, 4439–4449.
[51] C. Adamo, D. Jacquemin, *Chem. Soc. Rev.* **2013**, *42*, 845–856.
[52] Y. Zhao, D. G. Truhlar, *Theor. Chem. Acc.* **2008**, *120*, 215–241.
[53] M. J. Frisch, G. W. Trucks, H. B. Schlegel, G. E. Scuseria, M. A. Robb, J. R. Cheeseman, G. Scalmani, V. Barone, G. A. Petersson, H. Nakatsuji, X. Li, M. Caricato, A. V. Marenich, J. Bloino, B. G. Janesko, R. Gomperts, B. Mennucci, H. P. Hratchian, J. V. Ortiz, A. F. Izmaylov, J. L. Sonnenberg, D. Williams-Young, F. Ding, F. Lipparini, F. Egidi, J. Goings, B. Peng, A. Petrone, T. Henderson, D. Ranasinghe, V. G. Zakrzewski, J. Gao, N. Rega, G. Zheng, W. Liang, M. Hada, M. Ehara, K. Toyota, R. Fukuda, J. Hasegawa, M. Ishida, T. Nakajima, Y. Honda, O. Kitao, H. Nakai, T. Vreven, K. Throssell, J. E. Montgomery, J. A., Jr. Peralta, F. Ogliaro, M. J. Bearpark, J. J. Heyd, E. N. Brothers, K. N. Kudin, V. N. Staroverov, T. A. Keith, R. Kobayashi, K. Normand, J. Raghavachari, A. P. Rendell, J. C. Burant, S. S. Iyengar, J. Tomasi, M. Cossi, J. M. Millam, M. Klene, C. Adamo, R. Cammi, J. W. Ochterski, R. L. Martin, K. Morokuma, O. Farkas, J. B. Foresman and D. J. Fox, Gaussian16, revision B.01, Gaussian, Inc., Wallingford CT, **2016**.
[54] S. S. Patil, K. G. Thorat, R. Mallah, N. Sekar, *J. Fluoresc.* **2016**, *26*, 2187–2197.
[55] F. L. Hirshfeld, *Theor. Chem. Acc.* **1977**, *44*, 129–138.
[56] D. K. A. Phan Huu, R. Dhali, C. Pieroni, F. Di Maiolo, C. Sissa, F. Terenziani, A. Painelli, *Phys. Rev. Lett.* **2020**, *124*, 107401.
[57] R. Dhali, D. K. A. Phan Huu, F. Terenziani, C. Sissa, A. Painelli, *J. Chem. Phys.* **2021**, *154*, 134112.
[58] A. Painelli, F. Terenziani, *J. Phys. Chem. A* **2000**, *104*, 11041–11048.
[59] B. Boldrini, E. Cavalli, A. Painelli, F. Terenziani, *J. Phys. Chem. A* **2002**, *106*, 6286–6294.
[60] S. Sanyal, C. Sissa, F. Terenziani, S. K. Pati, A. Painelli, *Phys. Chem. Chem. Phys.* **2017**, *19*, 24979–24984.
[61] A. Painelli, *Chem. Phys. Lett.* **1998**, *285*, 352–358.
[62] A. Painelli, F. Terenziani, *Chem. Phys. Lett.* **1999**, *312*, 211–220.
[63] A. Painelli, L. Del Freo, F. Terenziani, *Chem. Phys. Lett.* **2001**, *346*, 470–478.

Manuscript received: March 28, 2023
Accepted manuscript online: May 19, 2023
Version of record online: July 13, 2023